



Determining the best places for dewatering wells in the Gohar-Zamin pit mine, using geostatistical methods

Beheshte Nakhaie Sarvedani ¹, Reza Jahanshahi ^{1,*}, Amin Assari ²

¹ Department of Geology, Faculty of Science, University of Sistan and Baluchestan, Zahedan, Iran

² Gohar-Zamin Iron Ore Co, Gol-Gohar Industrial & Mining, Iran

Received: 25 February 2022, Revised: 05 May 2022, Accepted: 18 May 2022

© University of Tehran

Abstract

The Gohar-Zamin mine is located in the southwest of Sirjan city in Kerman province, Iran. Geology condition showed that two fault categories played an important role in the formation of crushed and weathered regions in the southern part of the pit. The spatial analysis of the Lugeon variable indicated that the hydraulic conductivity in the rock mass is very low and the groundwater flow is concentrated only in a limited number of high-transmission main gaps. The mine needs to the designing a proper system for dewatering. Hence, a Gaussian simulation method was used to determine the suitable location of the dewatering wells in the vicinity of the pit. Exploratory spatial data analysis (ESDA) was used to examine location maps, histograms, correlations, and variogram of the Lugeon and RQD data. The relationship between Lugeon and RQD with depth demonstrated that the minimum of RQD and maximum of Lugeon were concentrated in certain elevations. The calculated variograms of RQD and Lugeon showed good spatial continuity. Variograms of the normalized values were performed to carry out the Gaussian simulation of the RQD and Lugeon variables. Probability and uncertainty maps of RQD and Lugeon indicated that the south-eastern parts of the pit play an important role in permeability.

Keywords: Permeability, Geostatistics, Lugeon, RQD, Sequential Gaussian Simulation.

Introduction

The groundwater inrush into the mine pit is one of the problems that can make extraction and mining activities difficult. The location and amount of water entering the mine pit are mainly dependent on the developed permeable zones within the formation of the region; therefore, in order to control the groundwater inrush and suggesting the best location of the pumping wells for the drainage of the mine, it is necessary that the zones and permeable areas identified. The permeable zones are usually identified using pumping test and evaluation of the lugeon and rock quality designation (RQD) data. Although the pumping test is the most accurate method to determine the permeability of rock mass, since the pumping test is costly, the most common method is lugeon or peck test (Alianvari et al., 2008).

The geostatistics methods are widely used to estimate the hydraulic parameters of the aquifer hydrogeological by geotechnical parameters. It has the advantage that it can be fully conditioned on all the available local information, even on indirect data such as hydraulic heads (De Marsily et al., 1998). This approach has widely been used in hydrogeological studies for estimation and simulation of hydraulic properties, e.g. transmissivity and hydraulic conductivity. Huysmans and Dassargues (2009) applied multiple-point geostatistics and variogram-based geostatistical methods to simulate permeability to determine the impact of

* Corresponding author e-mail: jahanshahireza@science.usb.ac.ir

complex geological heterogeneity on groundwater flow. Other studies include Jang and Liu (2004), Nowak and Cirpka (2006), Patriarche et al. (2005), and Soltani-Mohammadi and Hezarkhani (2013). Simulation is one method for modelling the geometry of the permeable layers (Jaquet et al., 2004). In this method, after analyzing spatial data, based on statistical parameters, the simulation of variables is performed. For geostatistical simulations, it is imperative to examine variograms of the spatially distributed variables and their characteristics, such as nugget and range, and then link them to the geological structures, such as bedding planes, faults, and joints (Assari et al., 2015). Geostatistical approaches have been studied worldwide (e.g. Assari and Mohammadi 2017; Madani Esfahani and Asghari 2012; Akhondi and Mohammadi 2014; Neuman et al., 1980; Assari and Mohammadi 2016; Razack and Iasm 2006; Marache et al., 2009; Triki et al., 2012; Boufekane et al., 2021; Narjary et al., 2021; Faria et al., 2021; Jalili Pirani 2020; Mallik et al., 2020; Zhang et al., 2020; Shojaei et al., 2018).

The Gohar-Zamin iron ore mine is one of the largest open pit mines in Iran (the central Iran structural zone). Groundwater seepage into the pit mine has created several problems, including slope instability, dewatering of blast holes, and mining operations below the groundwater table. Hydrogeology of the mine showed that during mining extraction, several boreholes intersected a pressurized zone and turned into flowing wells (Assari, 2019). Since the final level of the pit is 400 m below ground surface, it needs to design a proper system for dewatering. Therefore, according to study and simulation of geostatistical, the aims of this research are: (a) exploratory-spatial analysis of data using various tools, (b) Stochastic simulation of RQD parameter to determine porous zones, (c) Identification of permeable zones in the rock layer of the mine and (d) determining the best location of suggested dewatering wells in the hard rock of the mine.

Study area

The study area is located in the southwest of Sirjan city, Iran (Fig. 1) and includes the Gol-e-Gohar mining area (six open pit mines) and industrial complex. Gohar-Zamin mine (pit number 3), has the largest reserves among the others. The diameters of pit in the E–W and N–S directions are about 1,700 and 1,300 m, respectively. This pit consists of 12 benches with height of 15 m (from elevation of 1,735 m to 1,555 m asl) (Assari 2019). According to Sabzehei et al. (1997), this area that located in the Sanandaj-Sirjan Zone, consists mainly of metamorphic rock while surface geology involves mostly of young alluvial deposits and consolidated sediments of gravel (Fig. 1). In the walls of Gohar-Zamin pit mine, an alternation of these fine and coarse grained sediments is observed too (Assari 2019). Units of recrystallized limestone and marble with schist are located in the southern parts of the mine. The main structures of the study area are the Baghat thrust fault and Kheir-Abad strike-slip fault. The Baghat thrust fault with NW–SE trend and slope to the north-east, is located in the south-western of Gohar-Zamin mine. The Kheir-Abad fault with an N–S trend begins from the western of the Kheir-Abad playa and the southern end joins the Baghat thrust fault (Shojaei Baghini et al., 2020; Assari 2019; Jahanshahi and Zare 2017; Jahanshahi and Zare 2015, Jahanshahi et al., 2014). In addition, in the walls of the mine several minor faults cropping out. The normal and strike-slip faults are young while the reverse faults are old (Assari 2019). Generally, in the study area there are two major structural trends in the faults: (1) faults with E–W strike that are typically of a normal type and dip south; (2) faults with N–S strike that are mostly of strike-slip type and sometimes cause the displacement of E–W faults (Mohajjel and Pur-Faraj 2016).

Hydrogeology

Several hydrogeological and geophysical studies have been conducted in the study area.

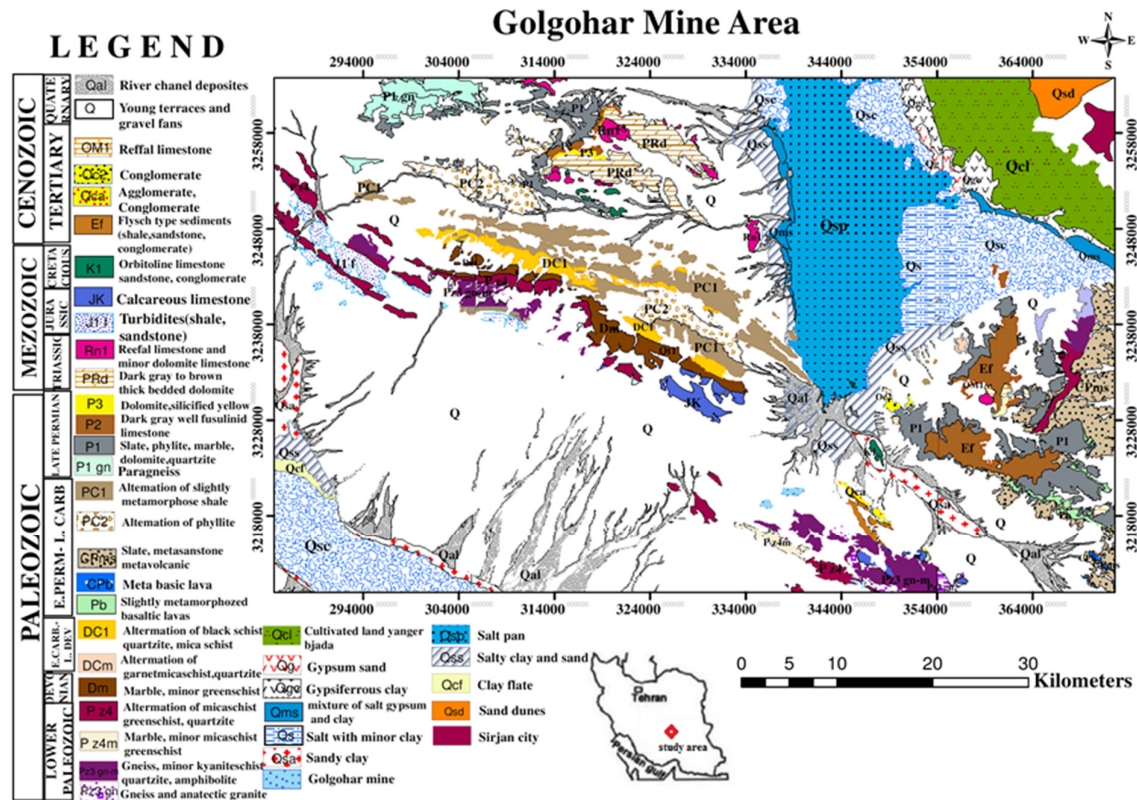


Figure 1. Geological map of Golgohar Sirjan Mineral Area

Previous studies showed that there are two main aquifers, which can be distinguished by criteria such as hydrochemical characteristics, hydraulic head, and lithology. In the GoharZamin mine area the maximum and minimum thickness of alluvium are 234.6 and 47.9 m, respectively (Assari 2019). There are also separate aquifers that are bounded from the bottom and top with impermeable layers; however, since the water table is below these layers; Therefore, they cannot be considered as confined aquifers (Assari 2019). Based on hydrochemical criteria, the lower hard rock aquifer has a higher EC (with a mean of 24.1 mS/cm); the upper aquifer, which is composed of alluvial deposits, has a lower EC (with a mean of 10.8 mS/cm). The lower aquifer also has higher transmissivity values (averaging 299.4 m²/d) compared to the upper aquifer (averaging 188.9 m²/d). The increased density of fracture zones with depth is likely the main reason for such variations in average transmissivity. Another important hydrogeologic parameter is the groundwater level, which is also different for the lower and upper aquifers (Assari 2019). The average groundwater level in the upper aquifer is 1685.11 m above sea level (asl), whereas it is 1681.87 m asl in the lower aquifer. All piezometers located within the pit showed large vertical hydraulic gradients, ranging from 0.046 to 0.730. The high values of the vertical hydraulic gradient are mainly attributed to the effect of pumping from the wells within the pit. Because of the high transmissivity of the lower aquifer, it is assumed that it mainly contributes to the discharge from the pumping wells (Assari 2019).

Materials and methods

Rock-quality designation (RQD) is a rough measure of the degree of jointing or fracture in a rock mass, measured as a percentage of the drill core in lengths of 10 cm or more. High-quality rock has an RQD of more than 75%, low quality of less than 50% (Mozafari et al., 2021). Rock

quality designation (RQD) is the borehole core recovery percentage incorporating only pieces of solid core that are longer than 100 mm in length measured along the centerline of the core. In this respect pieces of core that are not hard and sound should not be counted though they are 100 mm in length. RQD was originally introduced for use with core diameters of 54.7 mm (NX-size core). RQD is defined as the quotient:

$$\text{RQD} = (L_s/L_t) \times 100\% \quad (1)$$

L_s = Sum of length of core pieces that are > 100 mm (4 inches) measured along the centerline.

L_t = Total length of core run.

The Lugeon test, sometimes call also Packer test, is an in-situ testing method widely used to estimate the average hydraulic conductivity of rock mass (Mozafari et al., 2020). It is indeed in situ test of formation permeability performed by measuring the volume of water taken in a section of test hole when the interval is pressurized at given pressure (10 bars -150 psi). It is used primarily in variably permeable formations under evaluation of fracturing. The test is conducted in a portion of a borehole isolated by pneumatic packers. The water is injected into the isolated portion of the borehole using a slotted pipe which itself is bounded by the inflated packers. The packers can be inflated using a gas compressor on the surface, and so they can isolate and seal that portion of the borehole. A pressure transducer is also located in that portion to measure the pressure with a help of reading station on the surface ((Mozafari et al., 2018).

Isatis software was used to study the geostatistics and geostatistical simulation. Isatis code is unique among geostatistics software packages, as it provides the best interactive analysis of 2D and 3D data with variogram maps and fitting, as well as many estimation techniques (simple and ordinary kriging, indicator kriging, disjunctive kriging, uniform conditioning) and grade or geology stochastic conditional simulations (Roosevelt 2013).

In geostatistical studies, variogram of the variable should be determined. The variogram, $\gamma(h)$, is half the average squared difference between the paired data values (Issaks and Srivastava 1989):

$$\gamma(h) = \frac{1}{2N(h)} \sum_{(i,j) \in h} (v_i - v_j)^2 \quad (2)$$

where $\gamma(h)$ denotes the variogram for an interval lag distance class h ; $N(h)$ represents the number of pairs for an interval lag distance class h . The experimental variogram, $\gamma(h)$, is fitted a theoretical model, such as spherical, exponential, or Gaussian, to determine three parameters, including the nugget effect, the sill and the range. These models are defined as follows (Isaaks and Srivastava 1989).

Spherical model:

$$\begin{cases} \gamma(h) = c_0 + \left[1.5 \left(\frac{h}{a} \right) - 0.5 \left(\frac{h}{a} \right)^3 \right], & h \leq a \\ \gamma(h) = c_0 + c & h > a \end{cases} \quad (3)$$

Exponential model:

$$\gamma(h) = c_0 + c \left[1 - \exp \left(-3 \frac{h}{a} \right) \right] \quad (4)$$

Gaussian model:

$$\gamma(h) = c_0 + c \left[1 - \exp \left[- \left(\frac{3h}{a} \right)^2 \right] \right] \quad (5)$$

Sequential Gaussian simulation is a very fast and straightforward way because this modelling in each location requires solving only one kriging system in that location.

In this research, variables of rock-quality designation (RQD) and Lugeon were considered as the basic indicators in the analysis of permeability and rock quality.

Exploratory data analysis comprised the following steps:

(1) According to Isaaks and Srivastava (1989), to diminish the effect of special sampling on the

statistical variables, it is necessary to decluster the data. Therefore, method of cell-declustering was used for RQD and Lugeon data. Through an iterative procedure, best size of cell was selected for the calculations. Cells in range sizes of 1 to 5000 m were considered and weights were separately calculated for every data point in such a way that the mean values of the Lugeon and RQD and were minimized and maximized respectively.

(2) RQD and Lugeon data were converted to standard normal values by a Gaussian transformation.

(3) Preliminary statistics, location maps, histogram and variogram of the RQD and Lugeon were prepared for different lithologies, depths and locations parts of the study area using the Isatis software (Roosevelt 2013).

The data were converted to a standard normal value with a Normal score transformation, a change in the normal values of both the RQD and Lugeon variables was plotted and used to perform a sequential Gaussian simulation, Finally, the uncertainty of simulation was determined.

The sequential Gaussian simulation had been used to simulation of RQD and Lugeon. Therefore, simulation grid, origin network, number of nodes and size of cells in the directions X, Y and Z and its rotation angle to the north was determined. Dimensions of $25 \times 25 \times 10$ meter in the grids were considered for both RQD and Lugeon variables and finally hundred simulations for these variables were produced and then these simulations were combined to obtain an expected value and the probability of exceeding a threshold value for each cell.

Results and discussion

Exploratory data analysis

The lithological well-log data of 230 boreholes was available for inside and outside of the mine pit. From these boreholes, in 87 and 14 of them, RQD and Lugeon were measured respectively (Fig. 2).

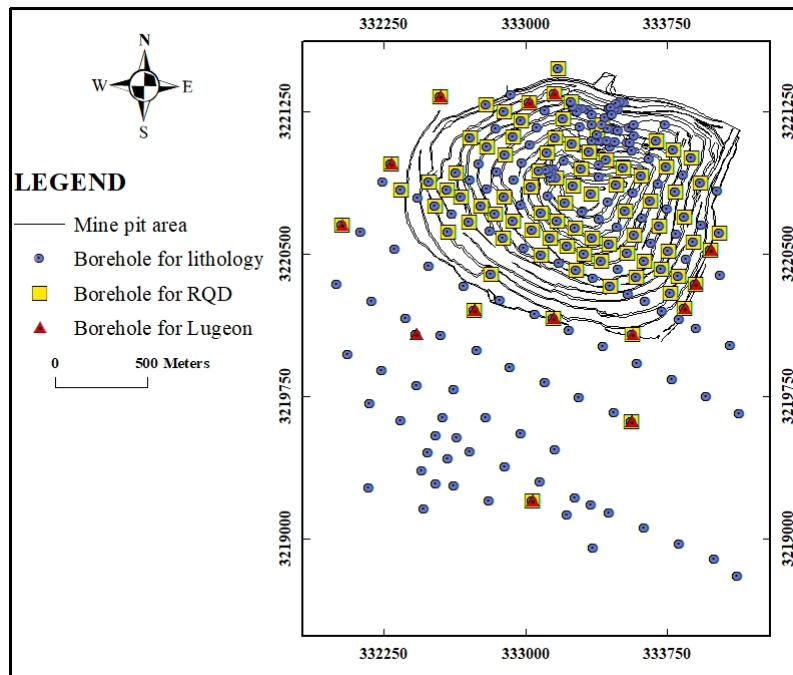


Figure 2. The location of various boreholes inside and outside of the Gohar-Zamin mine pit

The well-logs showed that lithology from up to down elevation in the boreholes generally include: dense layer of alluvium, amphibolite, bressia zone, chlorite schist, conglomerate, fault zone, gneiss, metabasite, quartz schist, skarn, oxidized magnetite, bottom magnetite and top magnetite.

A total of 5437 and 47 for RQD and Lugeon data were available respectively. From these RQD data, 4946 and 491 were measured in hard rock formations and the dense layer of alluvium respectively. Investigation and comparison of the omnidirectional variogram ($\gamma(h)$) in the dense alluvium layer and hard rock formation showed that the range of fitted variogram model for the hard rock formation was approximately three times more than that dense alluvium layer (Fig. 3). Therefore, due to this distinction, and simulation just for hard rock formation, data of the dense alluvial layer was omitted from the calculation process.

The cell declustering method was used to decluster the RQD and Lugeon variables. By applying the declustering weight, the histogram of RQD and Lugeon were generated (Fig. 4a and c). After declustering of data, values of mean, standard deviation and median for the RQD were increased from 39.08, 30.27 and 34.67 to 40.51, 30.73 and 36.3 respectively while those for Lugeon were reduced from 2.51, 3.49 and 1.55 to 1.80, 2.15 and 1.48 respectively. It indicated that applying weight to the data, has exacerbated non-compliance of data with normal distribution. In order to investigate the spatial continuity of these variables, omnidirectional variograms were used (Fig. 4b and d) and showed that RQD variable has a spatial continuity of up to 401 m while for the Lugeon, it was up to 800 m.

Correlation between variables

The correlation between variables of RQD, Lugeon and depth were examined to identify the relationship and the degree of dependence between them. The boxplot variation of RQD and Lugeon in the direction of depth indicated that with increasing the depth, a fluctuating trend was observed for RQD values, and high values of Lugeon was located at elevation level close to the ground surface.

In the study area, since the RQD data was more than the Lugeon, two criteria of the mean and minimum of data were considered in the correlation of the RQD and Lugeon. With regarding the scatter plot diagrams of minimum and mean values of RQD and Lugeon, it showed that a low correlation was observed between them (Fig. 5).

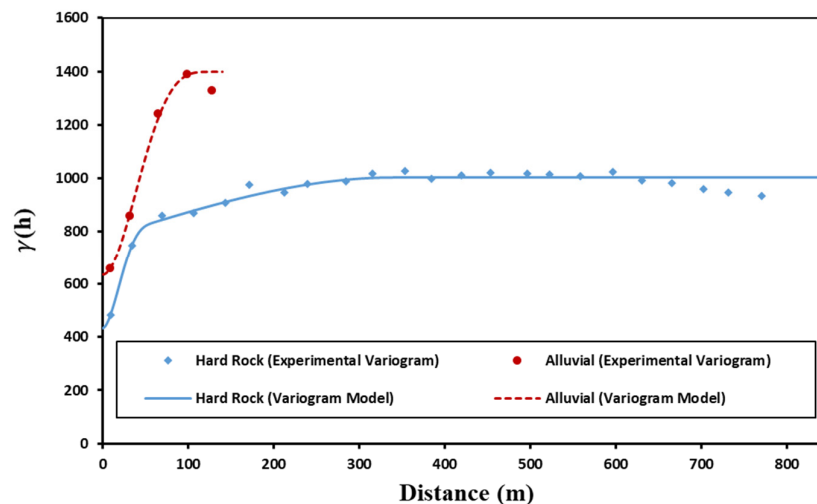


Figure 3. Comparison experimental variograms (points) and fitted variogram model (lines) for the dense alluvium and hard rock formation

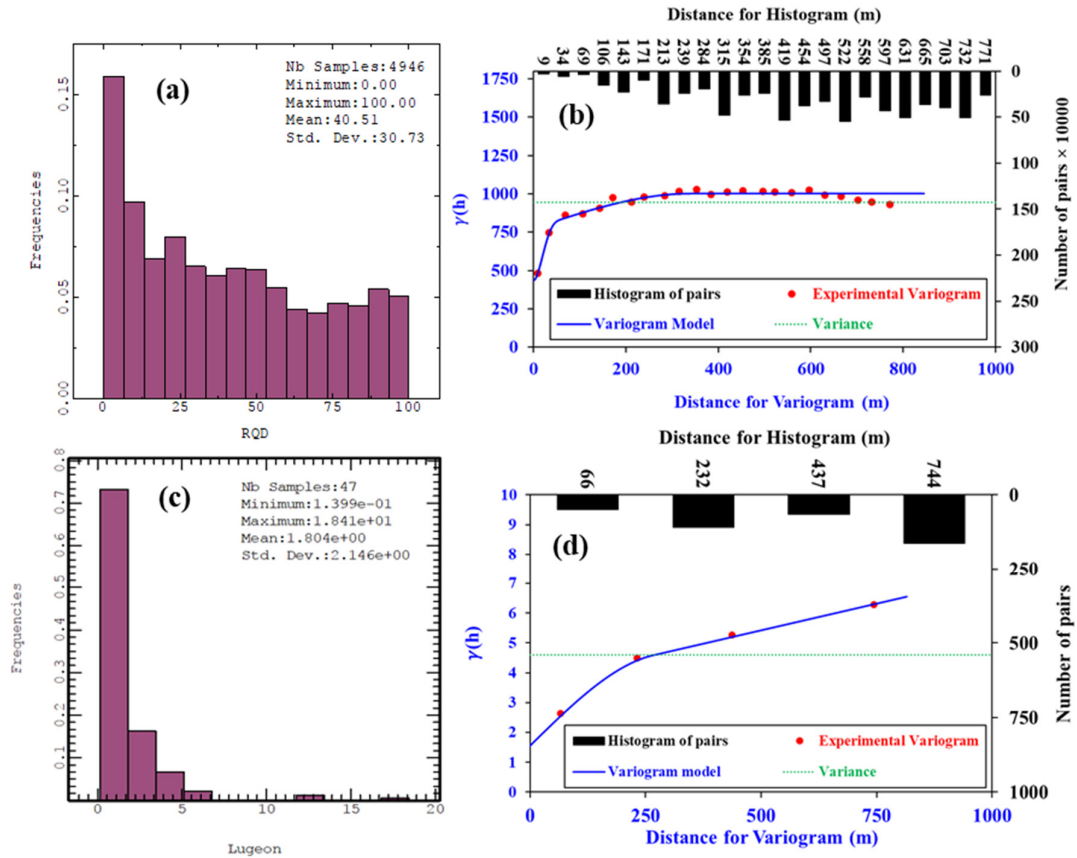


Figure 4. Histogram and omnidirectional variograms for RQD (a and b) and for Lugeon (c and d)

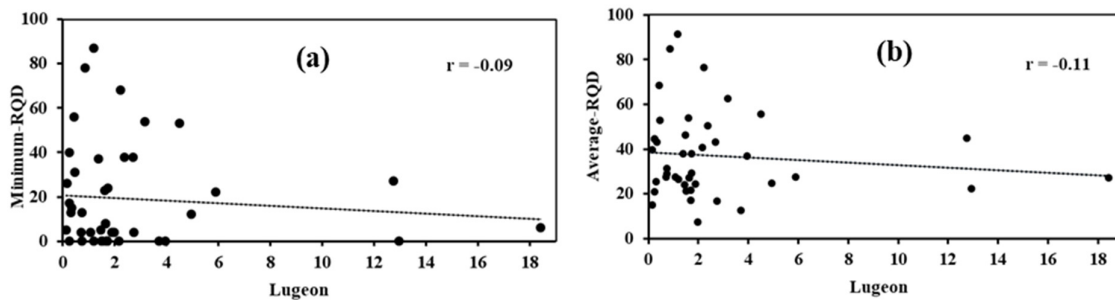


Figure 5. Correlation between minimum values (a) and average values (b) of RQD with Lugeon

However, this can be due to the different nature of the RQD and Lugeon variables. Because the RQD variable is generally measuring from a piece of rock with small size and it can be considered as a point variable while the amount of the Lugeon is representative of a value in area around the well. Therefore, the presence of a fracture that has a hydraulic relationship with the fractures and major cavities in the rock matrix can greatly increase the Lugeon value, whereas the same fracture may not have a large effect on the RQD variable. The opposite may also be the case; the RQD may show small value, but these fractures are localized and do not extend much into the surrounding rocks. In such a case, although the RQD is low, the values of high Lugeon are not obtained.

RQD in different lithology and elevations

To investigate the spatial continuity of the RQD variable in different lithology and altitudes

level, the experimental variogram were calculated and modelled for each of the lithology and altitudinal levels (Fig. 6 and 7). The variograms of lithology showed that Amphibolite, Bottom magnetite, Bressia zone, and Quartz schist lithology had high spatial continuity. The Gneiss lithology had a very small spatial continuity up to 30 m. It seems that a very weak hole effect existence in an approximate distance 18-40 m, which indicates changes in this variable at low intervals and it may be due to the effect of faults and weathered layer. Lithology of Conglomerate, Skarn and Oxidized magnetite had a moderate spatial continuity while Chlorite schist had a low spatial continuity (Fig. 6).

The RQD variogram for various elevations showed that levels of 1250 to 1450 m had lowest spatial continuity due to lower data range. Additionally, at level of 1250- 115 m, the nugget effect was high that resulted from more intense changes on a small scale; therefore, in deeper sections, the amount of heterogeneity increases and the changes become more intense.

The experimental variogram were also computed for various lithology and elevations. Results showed that various lithologies have different spatial continuities and that this makes the pattern of spatial continuity more specific.

To simulation and estimation, it needs to the variogram (or covariance function) for different directions in the three-dimensional space. For the RQD variable, the three directions of azimuth 0-dip 0, azimuth 90-dip 0 and dip 90 had best spatial continuity; Therefore, the three directions were combined and a single model was fitted to them (Fig. 8a), and this model was used for sequential Gaussian simulation. Four models of nugget effect, cubic, spherical and power were applied to fitting on the experimental variograms (Table 1). Regarding the three-directional variogram of the normal values of the RQD variable, the east-west direction had the highest spatial continuity relative to the two north-south directions and the vertical direction. In addition to spatial continuity in the north-south direction was more than the vertical direction.

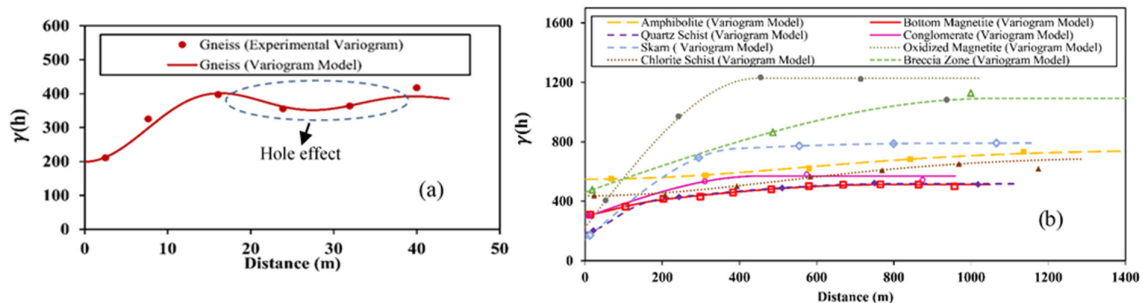


Figure 6. The RQD experimental variograms and fitted variogram model for (a) Gneiss lithology and (b) lithology of Amphibolites, Bottom Magnetite, Quartz Schist, Conglomerate, Skarn, Oxidized Magnetite, Bressia zones and Chloritic Schist

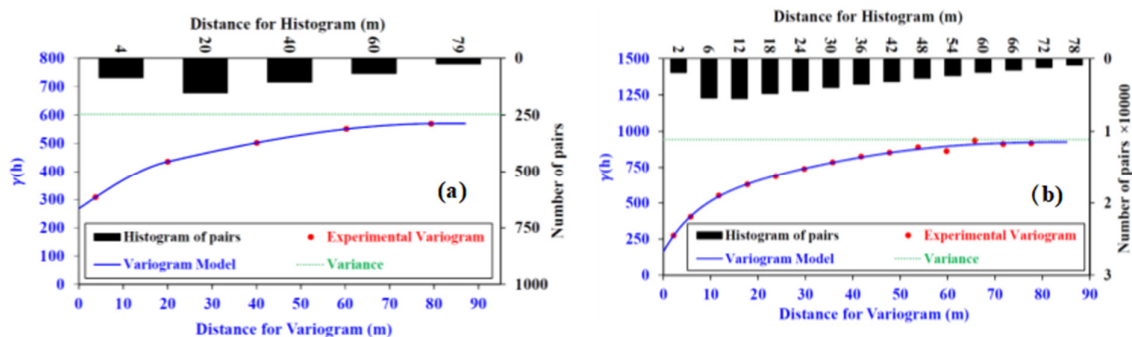


Figure 7. The RQD experimental variograms and fitted variogram model for various height levels, (a) 1150-1250 m, (b) 1550-1650 m

Table 1. Specifications of the fitted unique model on the experimental variogram in the three perpendicular directions (dip 90; azimuth 90; Dip 0; azimuth 0; dip 0) for normalized RQD values

Variable	Variogram	Model	Range (meter)	Model weight	Sum of Squared Residuals (SSR)
RQD	Unique variogram	Nugget effect	-	0.3	0.0006
		Cubic	(2.5, 100.7, 49703.7)	0.18	
		Spherical	(354.4, 270.8, 35.9)	0.4	
		Exponential	(151.4, 59073.0, 3273.3)	0.12	

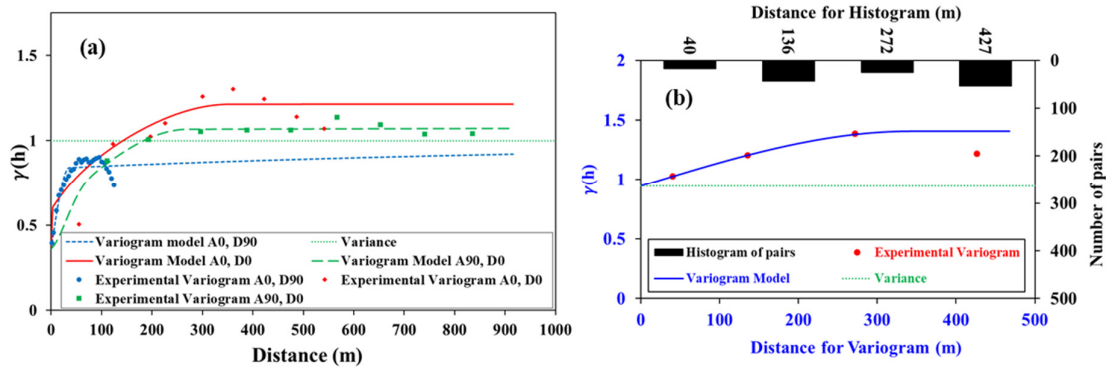


Figure 8. The Lugeon experimental variogram and fitted variogram unique model for normalized RQD data in directions of azimuth 0 and Dip 0, azimuth 90 and Dip 0, and Dip 90 (a) and normalized data (b)

The variogram of the normalized Lugeon values in different directions showed that there was no trend in the spatial continuity. Hence sequential Gaussian simulation was performed using an omnidirectional variogram of the normalized values. Two models of nugget effect and spherical were fitted on the experimental variogram (Fig. 8b). The spatial continuity calculated 341 m and the nugget effect was 0.94 that indicated a high variation of Lugeon exist in short distances.

Sequential Gaussian Simulation

In order to investigate the uncertainty of simulations and determine of the suitable areas for drilling wells, the average of probabilities was calculated between final level of pit bottom (1297 m) and the boundary between alluvium and hard rock (1650 m). The uncertainty map of the RQD variable (Fig. 9a) indicates the mean of probability of RQD with values less than the threshold of 30. According to this Figure, southeast, southwest and west of pit were the best places to suggestion for drilling wells in mine dewatering plan.

The Lugeon variable uncertainty map has been shown in Fig. 9b. Lugeon value 2 was chosen to examine the risk maps and uncertainties. According to the uncertainty map the probability of Lugeon more than 2 located in the southeast, south, and northwest of the pit. If this map is compared with the map of the probability of RQD less than 30 (Fig. 9a), it can be observed that in some areas there is good agreement between low values of RQD and high values of Lugeon. For example, in the south-eastern part of the pit, probability values reach the maximum for both RQD and Lugeon. The correlation curve between the mean probability of the two variables in the south-eastern of the pit presented in Fig. 9d. By comparing this Figure with Fig. 5, it can be clearly identified that the correlation coefficient between two variables changed from a low ($r = -0.11$ and -0.09) values in the whole region to a positive and high correlation coefficient ($r = 0.88$) in the south-eastern part. Therefore, this high correlation confirmed the present of a permeable or crushed zones in this area.

In some places, including northwest and western parts of the mine, the trend of changes in the probability values of RQD and Lugeon was not consistent with each other.

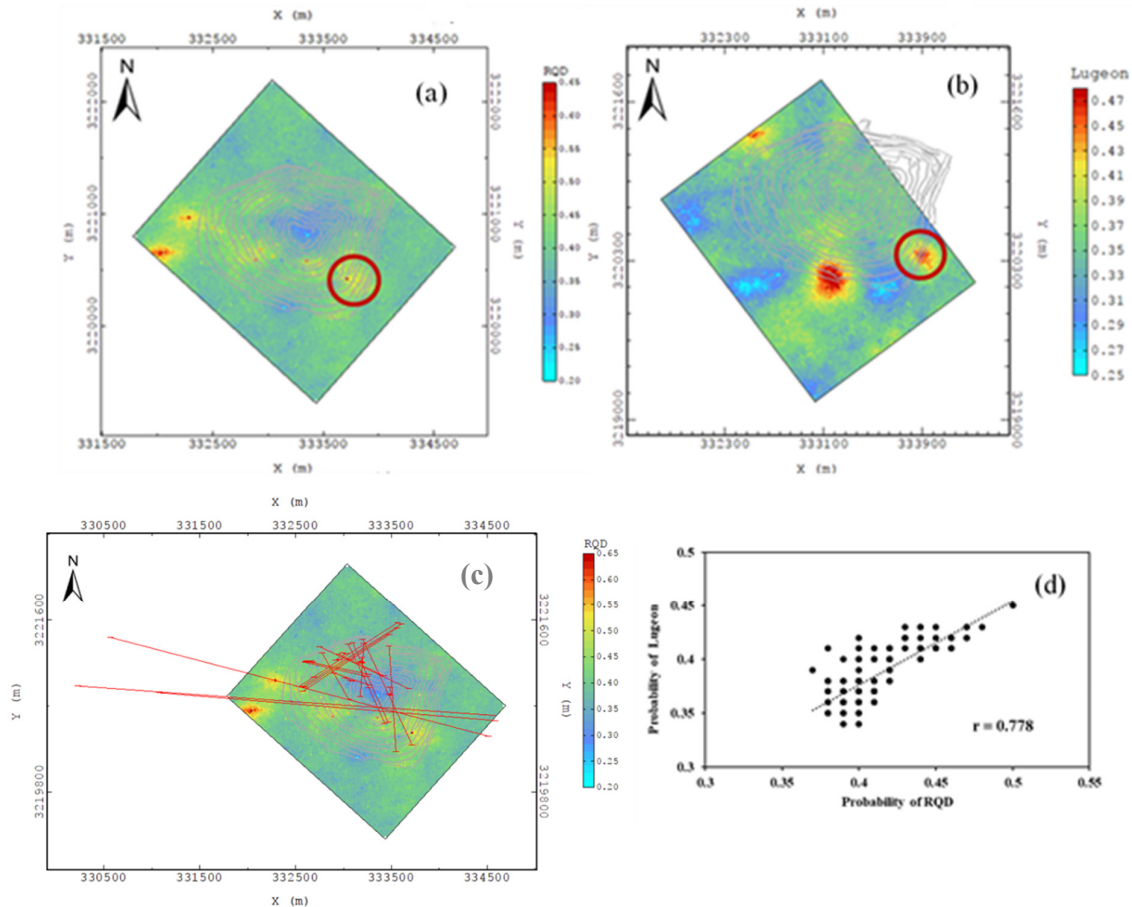


Figure 9. Map of the mean probability of RQD less than 30 (a) and Lugeon greater than 2 (b) correlation between the mean probability of the RQD and Lugeon in the southeastern of the pit (c) and matching of the faults on the map of the mean probability of RQD less than 30 for final level of the pit to boundary between the dense alluvium layer (d).

Therefore, it is necessary to consider both maps in order to decide about determination of the location of pumping wells. However, since the data used in RQD simulation was much more than the number of Lugeon data, it is recommended that the map of the probability values of RQD be placed in the first priority.

In order to investigate the relationship between faults and crushed zones, the position of the strike-slip faults was plotted on uncertainty map of RQD values (Fig. 9c). Two main strike-slip faults with an almost northwest-southeast and eastern-western trend are extending from the southern part of the pit and located almost along with the position of the permeable zones. Nonetheless a few deviations are observed, and these deviations may be due to the lack of precise knowledge of the faults process. The map also showed only the average of available probabilities and does not fit perfectly with what is present in reality.

Conclusion

Geology condition showed that two fault categories played an important role in the formation of crushed and weathered regions in the southern part of the pit. The spatial analysis of the Lugeon variable indicated that the hydraulic conductivity in the rock mass is very low and the groundwater flow is concentrated only in a limited number of high-transmission main gaps. Investigating the probability of RQD values and uncertainty maps of the mine area pit indicated

that the south-eastern, south-western, and western of the pit were most likely to be low in terms of the RQD and hence high permeability. While, for Lugeon, high values of the hydraulic conductivity were located in the south-eastern, southern and north-western of the pit. The geostatistical simulation was indicated south-eastern of the pit had the most important role in permeability and as a result of the groundwater movement toward pit; therefore, this area is considered as the priority of the location for pumping wells for pit drainage.

Acknowledgments

The authors would like to thank the Gohar-Zamin Iron Ore Company.

References

- Aali Anuri, A., Katibeh, H., Mahmoudabadi, H., 2008. Equivalence of permeability estimation along Amirkabir tunnel axis using artificial neural network, 2nd Iranian Conference on Mining Engineering, Tehran, University of Tehran.
- Aghanbati, S.A., 2004. Geology of Iran, Tehran, Geological Survey of Iran.
- Akhondi, M., Mohammadi, Z., 2014. Preliminary analysis of spatial development of karst using a geostatistical simulation approach. *Bull of Eng Geo and the Env.* 73(4):1037-1047, 2014.
- Assari, A., 2016. Conceptual model of groundwater in the area of Goharzamin mine. Goharzamin iron ore company.
- Assari, A., 2019. Defining hydrogeology of the Gohar-Zamin open pit mine, Iran: a case study in a hard-rock aquifer. *Hydrogeology J.* 27(4):1479-1495.
- Assari, A., Mohammadi, Z., 2016. Analysis of rock quality designation (RQD) and Lugeon values in a karstic formation using the sequential indicator simulation approach, Karun IV Dam site, Iran. *Bull of Eng Geo and the Env.* 76(2):1-12.
- Assari, A., Mohammadi, Z., Namdar Ghanbari, R., 2015. Local variation of hydrogeological characteristics in the Asmari karstic limestone at the Karun IV Dam, Zagros region, Iran. *Quarterly J of Eng Geo and Hydrogeo.* 49(1):105-115.
- Boufekane, A., Yahiaoui, S., Meddi, H., Meddi, M., Busico, G., 2021. Modified DRASTIC index model for groundwater vulnerability mapping using geostatistic methods and GIS in the Mitidja plain area (Algeria). *Env Forensics.* doi.org/10.1080/15275922.2021.1913674
- Darvishzadeh, A., 1991. Geology of Iran, Tehran, Amirkabir Publications.
- De Marsily, G., Delay, F., Teles, V., Schafmeister, M., 1998. Some current methods to represent the heterogeneity of natural media in hydrogeology. *Hydrogeol J.* 6:115-130
- Faria, P.H., Coimbra Leite Costa, J.F., Arcari Bassani, M.A., 2021. Multivariate geostatistical simulation with PPMT: an application for uncertainty measurement. *App Earth Sci.* 130(3):174-184.
- Goovaerts, P., 1997. Geostatistics for natural resources evaluation, Oxford University Press, New York.
- Houlsby, A., 1976. Routine Interpretation of the Lugeon water test. *Q J Eng Geol.* 9:303-313.
- Huysmans, M., Dassargues, A., 2009. Application of multiple-point geostatistics on modelling groundwater flow and transport in a cross-bedded aquifer (Belgium). *Hydrogeol J.* 17:1901-1911
- Jahanshahi, R., Zare, M., 2015. Assessment of heavy metals pollution in groundwater of Golgohar iron ore mine area, Iran. *Environ Earth Sci.* 74(1):505-520.
- Jahanshahi, R., Zare, M., 2017. Delineating the Origin of Groundwater in the Golgohar Mine Area of Iran Using Stable Isotopes of 2H and 18O and Hydrochemistry. *Mine Water and the Env.* 36(4):550-563
- Jahanshahi, R., Zare, M., Schneider, M., 2014. A Metal Sorption/Desorption Study to Assess the Potential Efficiency of a Tailings Dam at the Golgohar Iron Ore Mine, Iran. *Mine Water and the Env.* 33(3):228-240.
- Jalili Pirani, F., Modarres, R., 2020. Geostatistical and deterministic methods for rainfall interpolation in the Zayandeh Rud basin, Iran. *Hydrological Sciences J.* 65(16):2678-2692.
- Jang, C.S., Liu, C.W., 2004. Geostatistical analysis and conditional simulation for estimating the spatial variability of hydraulic conductivity in the Choushui River alluvial fan, Taiwan. *Hydrol Process.* 18:1333-1350
- Jaquet, O., Siegel, P., Klubertanz, G., Benabderrhamane, H., 2004. Stochastic discrete model of karstic

- networks. *Advances in Water Res.* 27 (7):751-760.
- Madani Esfahani, N., Asghari, O., 2012. Fault detection in 3D by sequential Gaussian simulation of Rock Quality Designation (RQD). *Arabian J of Geo.* 6(10):3737-3747.
- Mallik, S., Bhowmik, T., Mishra, U., Paul, N., 2020. Mapping and prediction of soil organic carbon by an advanced geostatistical technique using remote sensing and terrain data. *Geocarto International*, doi.org/10.1080/10106049.2020.1815864.
- Marache, A., Breyse, D., Piette, C., Thierry, P., 2009. Geotechnical modeling at the city scale using statistical and geostatistical tools: the Pessac case (France). *Engineering Geo.* 107(3-4):67-76.
- Mozafar, M., Milanović, P., Jamei, J., 2021. Water leakage problems at the Tangab Dam Reservoir (SW Iran), case study of the complexities of dams on karst. *Bulletin of Engineering Geology and the Environment.* 80:7989-8007.
- Mozafari, M., Raeisi, Ezzat., Guerrero, J., 2018. Contribution of spectral coherency analysis and tracer test to study leakage at the Doosti Dam reservoir, Iran and Turkmenistan. *Environmental Earth Sciences.* 77:139.
- Mozafari, M., Sajjadian, M., Sorninia, Y., Bagheri, R., Ghader, Fatemeh., 2020. Hydrogeology and geomorphology of Bisetun Aquifer (NW Iran): interesting example of deep endokarst. *Carbonates and Evaporites.* 35:115.
- Mucke, A., Younessi, R., 1994. Magnetite-apatite deposits (kiruna type) along the sanandaj-sirjan zone and in the Bafq area, Iran, associated with ultramafic and calcalkaline rocks and carbonatites. *Mineralogy and Petr.* 50(4):219-244.
- Narjary, B., Kumar, S., Meena, M., Kamra, S.K., Sharma, D.K., 2021. Spatio-temporal mapping and analysis of soil salinity: An integrated approach through Electromagnetic induction (EMI), multivariate and geostatistical techniques. *Geocarto International*. doi.org/10.1080/10106049.2021.2002952
- Neuman, S.P., Fogg, G.E., Jacobson, E.A., 1980. A statistical approach to the inverse problem of aquifer hydrology: 2. Case study. *Water Resources Res.* 16(1):33-58.
- Nonveiller, E., 1989. *Grouting in theory and practice*. Elsevier Science Ltd., Amsterdam. 250 p.
- Nowak, W., Cirkpa, OA., 2006. Geostatistical inference of hydraulic conductivity and dispersivities from hydraulic heads and tracer data. *Water Resour Res.* 42(8): W08416, 6.
- Patriarche, D., Castro, MC., Goovaerts, P., 2005. Estimating regional hydraulic conductivity fields—a comparative study of geostatistical methods. *Math Geol.* 37:587-613.
- Razack, M., Lasm, T., 2006. Geostatistical estimation of the transmissivity in a highly fractured metamorphic and crystalline aquifer (Man-Danane Region, Western Ivory Coast). *J of Hydrology.* 325 (1-4):164-178.
- Roosevelt, F., Isatis., 2013. *Beginner's Guide, Geostatistics*.
- Shademan khakestar, M., Hassani, H., Moarefvand, P., Madani, H., 2016. Prediction of the collapsing risk of mining slopes based on geostatistical interpretation of geotechnical parameter. *J of the Geological Soc of India.* 87(1):97-104.
- Shojaei, S., Jahanshahi, R., Mali, S., Nasiri, M.A., 2020. Destruction of groundwater quality and the risk of saltwater intrusion in the aquifers nearby Sirjan salt playa, Iran. *Inte J of Env Analytical Chemistry.* 100(6):647-661.
- Shojaei, S.R.H., Waghei, Y., Mohammadzadeh, M., 2018. Geostatistical analysis of disease data: a case study of tuberculosis incidence in Iran. *J of Applied Statistics.* 45(8):1476-1483.
- Soltani-Mohammadi, S., Hezarkhani, A., 2013. A simulated annealing based algorithm to locate additional drillholes for maximizing the realistic value of information. *Nat Resour Res.* 22:229-237
- Triki, L., Zairi, M., Ben Dhia, H., 2012. A geostatistical approach for groundwater head monitoring network optimisation: case of the Sfax superficial aquifer (Tunisia), *Water and Env. J.* 27(3):362-372.
- Zhang, W., Wang, S., Song, S., Tan, C., Ma, Z., Shan, B., Xu, P., 2020. Determination of representative volume element with consideration of linear anisotropy using geostatistics approach. *European J of Env and Civil Engineering.* doi.org/10.1080/19648189.2020.1815588.

